Near-Infrared Imaging Hot Paper

DOI: 10.1002/anie.201307346

Biological Imaging Using Nanoparticles of Small Organic Molecules with Fluorescence Emission at Wavelengths Longer than 1000 nm**

*Zhimin Tao, Guosong Hong, Chihiro Shinji, Changxin Chen, Shuo Diao, Alexander L. Antaris, Bo Zhang, Yingping Zou, and Hongjie Dai**

Traditional near-infrared (NIR) imaging in the 750–800 nm region has been widely used for biological research and biomedical applications over the past decades. NIR imaging has advantages over imaging in the visible range because of reduced optical absorption and lower autofluorescence of biological substances.[1,2] Nowadays, many fluorophores exist for imaging in the visible range, and an increasing number of NIR fluorophores have become commercially available as a result of decades of research on fluorophores;[3–6] indocyanine green (ICG) was the first NIR fluorophore to be approved for use in humans by the US Food and Drug Administration (FDA). ICG is a water-soluble tricarbocyanine dye that emits at approximately 800 nm in the NIR region and can be safely intravenously administered to humans.[7]

Recently, we and others have found that fluorescent probes that emit at longer wavelengths in a new NIR-II window (1.0–1.7 μm) are advantageous for biological imaging, mainly because of greatly reduced photon scattering by the tissue.[8–20] Prior to these efforts, the NIR-II window had rarely been used for biological imaging, as no biocompatible fluorophores had existed that emit at wavelengths greater than 1000 nm, and because a borderline exists at approximately 1000 nm that separates the detection ranges of commonly used silicon photodetectors and cameras from those of their lower-band-gap semiconductor counterparts. The benefit of significantly reduced photon scattering outweighs the disadvantage of slightly increased light absorption in the NIR-II window, as it enables in vivo fluorescent imaging with higher spatial resolution at much greater penetration depths (several millimeters) than traditional NIR fluorescence imaging (<1 mm) with whole animals.[11]

Inorganic carbon nanotubes,[8–15] several quantum dots (e.g., Ag_2S, Ag_2Se, InSb),[16–19] and rare-earth nanoparticles[20] are the only fluorescent probes that have been used for biological imaging in the NIR-II region thus far. Therefore, it would be desirable to develop or synthesize small organic molecules that emit at wavelengths greater than 1000 nm to build a much larger library of NIR-II fluorophores, as has previously been done for the visible and traditional NIR windows. Approaches that employ small organic molecules are most likely to eventually satisfy all of the characteristics desired for NIR-II fluorophores, including a high quantum yield (QY), high biocompatibility, and rapid excretion from animals and humans. Currently, there are only a small number of organic molecules that are known to fluoresce in the >1000 nm region, all of which are highly hydrophobic, water-insoluble cyanine or thiopyrilium dyes, including IR-26, IR-1048, IR-1051, and IR-1061.[21–24] In their native forms, none of these organic dyes have been used or are suitable for biological imaging in the NIR-II window.

Herein, we report the synthesis of the first biocompatible NIR-II agent, which is based on the organic dye IR-1061, for in vivo imaging. IR-1061 is a commercially available water-insoluble polymethine dye (Figure 1a). IR-1061 is only soluble in several organic solvents, including dichloromethane (DCM) and 1,2-dichloroethane (DCE). The fluorescence quantum efficiency of IR-1061 is not well described; in one study, it was determined to be approximately (1.7 ± 0.5) % in

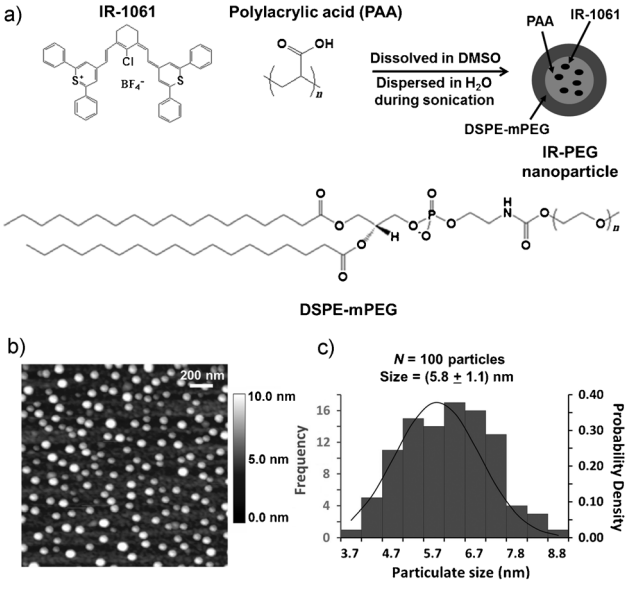

Figure 1. Synthesis of biocompatible IR-PEG nanoparticles with fluorescence emission >1000 nm. a) Synthetic procedure for IR-PEG nanoparticles from IR-1061 embedded in a poly(acrylic acid) matrix coated with PEGylated phospholipids (DSPE-mPEG). b) AFM image of the synthesized nanoparticles deposited on a silicon substrate. c) Topographic height histogram that shows the size distribution of ca. 100 randomly selected nanoparticles.

[*] Dr. Z. Tao,[+] G. Hong,[+] C. Shinji, Dr. C. Chen, S. Diao, A. L. Antaris, B. Zhang, Dr. Y. Zou, Prof. H. Dai
Department of Chemistry, Stanford University
Stanford, CA 94305 (USA)
E-mail: hdai@stanford.edu

[+] These authors contributed equally to this work.

[**] G.H. is thankful for a William S. Johnson Fellowship.

Supporting information for this article, including experimental details, is available on the WWW under http://dx.doi.org/10.1002/anie.201307346.

DCM by using rhodamine B in ethanol as a reference system (emission below 800 nm).[24] To make IR-1061 water-soluble, it was mixed with the amphiphilic polymer poly(acrylic acid) (PAA) to form nanoparticles with IR-1061 embedded in the PAA matrix; these nanoparticles were then coated with the surfactant DSPE-mPEG (a polyethylene glycol-conjugated phospholipid, ca. 5 kDa; Figure 1a). This approach is motivated by combining organic dyes and conjugated polymers to develop biocompatible imaging agents for the <800 nm window.[25–31]

The IR-PEG nanoparticles were prepared through a one-pot synthesis. First, IR-1061 and PAA were dissolved in dimethyl sulfoxide (DMSO) and then quickly added to a DSPE-mPEG aqueous solution, which was followed by sonication of the solution. DMSO and any unreacted reagents were removed from the mixture by centrifugal filtration (molecular weight cut-off: 100 kDa). The IR-PEG nanoparticles were re-dissolved in water, repeatedly washed, and centrifuged to remove any precipitates (see the Supporting Information for details).

Atomic force microscopy (AFM) was employed to image IR-PEG nanoparticles deposited on a silicon substrate. Uniformly sized nanoparticles were observed (Figure 1b), and a histogram of the topographic height of the nanoparticles (Figure 1c) revealed a mean diameter of about 5.8 nm with a standard deviation of 1.1 nm. The mass ratio of all reactants was IR-1061/PAA/DSPE-mPEG = 0.08:1:20 (molar ratios: 1.1:5:40). Excess surfactant was removed by centrifugal filtration, and approximately 54% of the DSPE-mPEG surfactant remained in the IR-PEG nanoparticles.

The formation of IR-PEG nanoparticles occurred when PAA and IR-1061 dissolved in DMSO were rapidly dispersed into water that contained the phospholipid-PEG surfactant. As DMSO mixed with water, the hydrophobic IR-1061 molecules were bound to and embedded into the hydrophobic parts of the PAA chains so that they could avoid contact with the aqueous phase, which led to the formation of nanoparticles. These nanoparticles were further wrapped by amphiphilic polymers to form aqueous stable complexes with the hydrophilic arm of the PEG chains extending into the aqueous surroundings. PAA is an excellent polydentate polymer for the functionalization of nanomaterials and is biocompatible.[32–34] We and others have shown that non-covalent coating of nanoparticles, including carbon nanotubes, with PEGylated phospholipids effectively stabilizes the nanoparticles in aqueous solutions, including sera and blood, reduces non-specific binding of biomolecules (e.g., proteins), and imparts biocompatibility for their use in vitro and in vivo.[8–11,13–17,35]

Free IR-1061 molecules dissolved in DMSO showed an absorbance peak at 1074 nm with a shoulder peak at 945 nm. IR-PEG nanoparticles in water exhibited blue-shifted absorbance, with a sharp peak at 780 nm and a shoulder peak at 1047 nm, which is caused by a different local environment of the IR-1061 molecules in the PAA matrix compared with that in DMSO. The blue-shift in the absorbance for IR-PEG nanoparticles in water brings the resonance absorption closer to the 808 nm laser line that is used for NIR-II imaging.[8–11,13–17] Fluorescence emission spectroscopy under

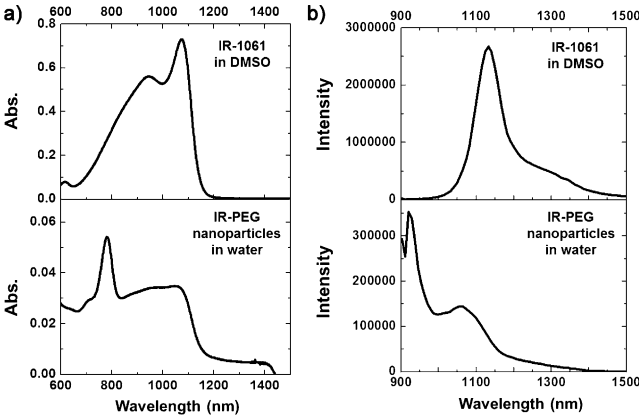

Figure 2. a) UV/Vis/NIR absorption spectra (600–1500 nm) and b) NIR-II fluorescence spectra (excited by an 808 nm laser) of free IR-1061 molecules in DMSO (top) and of IR-PEG nanoparticles in water (bottom).

808 nm laser excitation revealed an emission peak for free IR-1061 in DMSO at 1132 nm (Figure 2b), whereas the emission spectrum of IR-PEG nanoparticles in water was blue-shifted (in accordance with the absorption spectra), with a major peak at 920 nm and a shoulder peak at 1064 nm. Similar results were also observed under 980 nm laser excitation (Supporting Information, Figure S1). However, the absorption and emission intensities of the free IR-1061 dye in DMSO were found to decay rapidly after dissolution. In fact, polymer embedment stabilized the optical properties of IR-1061 in both DMSO and water.

The fluorescence QY of IR-PEG nanoparticles in water in the NIR-II region was measured to be approximately 1.8% by using IR-26 molecules in DCE as the reference system (QY of IR-26 $\approx$ 0.5%; see the Supporting Information and Figure S2 for details of the QY measurements).[36,37] This QY was higher than that of unseparated carbon nanotubes (ca. 0.4%), but lower than that of Ag_2S quantum dots (ca. 15%).[17] Importantly, IR-PEG nanoparticles in aqueous solutions exhibited higher photostability than free IR-1061 in DMSO, and retained an emission intensity of 85% under continuous laser excitation/illumination for one hour (Figure S3). These results suggest that an NIR-II fluorescent agent that is based on small organic molecules and stable under aqueous conditions was successfully prepared.

Next, we performed whole-body imaging of nude mice after intravenous injection of a solution (200 μL) of IR-PEG nanoparticles in phosphate-buffered saline (PBS; Movie S1), at an injected dose of approximately 0.27 mg mL^{-1} (based on the mass of IR-1061 embedded in PAA; ca. 360 μM of IR-1061). Video-rate imaging at 8.4 frames per second was applied to take advantage of the relatively high QY of the IR-PEG nanoparticles. Within approximately 4 s after injection, fluorescence of the IR-PEG nanoparticles in the lungs and kidneys of the mouse was observed as the nanoparticles passed through these organs with the blood flow (Figure 3a,b), before entering other parts of the mouse (Figure 3c). Video-rate imaging (Movie S1) and still images (Figure 3) immediately taken after injection indicated

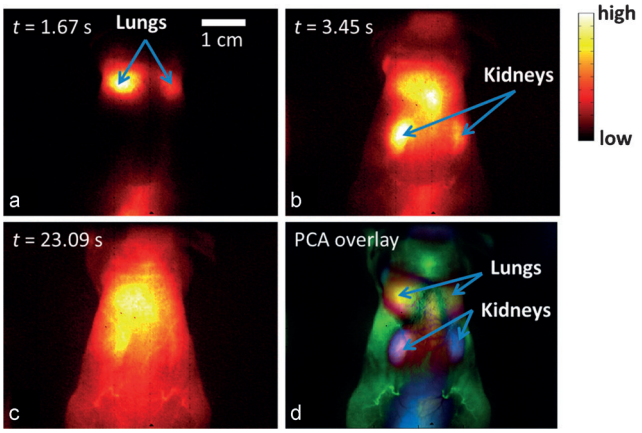

Figure 3. a–c) In vivo NIR-II imaging of a nude mouse with intravenously injected IR-PEG nanoparticles. NIR-II fluorescence images of the entire body of the mouse were recorded at various times after injection of the IR-PEG nanoparticles into the mouse tail vein. d) PCA-overlaid image based on the first 200 consecutive images of video-rate NIR-II imaging.

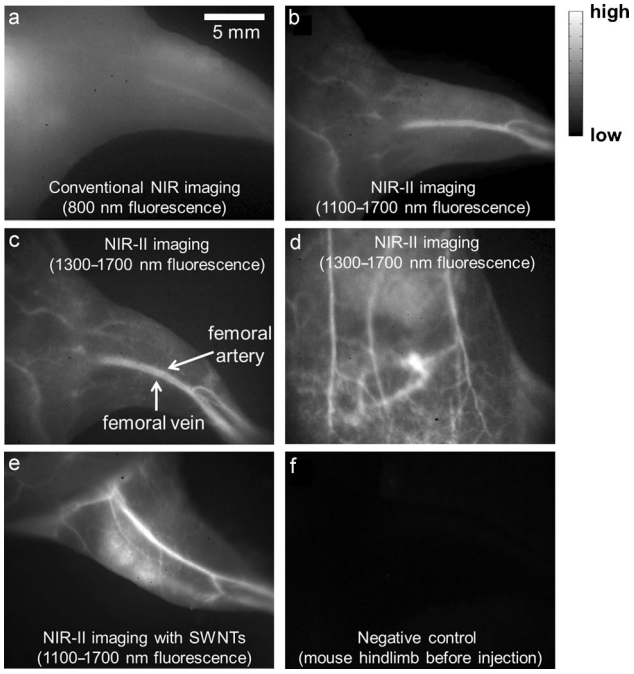

Figure 4. In vivo NIR imaging of the hindlimb and abdomen of nude mice with fluorophores circulating in the blood streams after intravenous injection. a) Image of a mouse hindlimb taken in the NIR window at ca. 800 nm after IRDye 800 injection (for details, see the Supporting Information). b, c) Images recorded after injection of IR-PEG nanoparticles under 808 nm laser excitation in the 1.1–1.7 μm and 1.3–1.7 μm NIR-II regions, respectively. d) An NIR-II fluorescence image of the abdomen taken in the 1.3–1.7 μm NIR-II region under 980 nm laser excitation after injection of IR-PEG nanoparticles. e) Image of a mouse hindlimb taken in the 1.1–1.7 μm NIR-II region after injection of single-walled carbon nanotubes under 808 nm laser excitation. f) Image of a mouse hindlimb taken in the 1.1–1.7 μm NIR-II region without injection of any fluorophores, thus showing minimal autofluorescence.

steady perfusion through the body without vessel occlusion. We were able to clearly image the blood flow through the hindlimb artery of the mouse seconds after injection. Based on the time-dependent variation of the NIR-II fluorescence throughout the body, we applied principal component analysis (PCA) to convert the time-dependent variation of the fluorescence intensity at various locations into spatially resolved components.[10,38] PCA combines image pixels with a similar time dependence into a distinct principal component and assigns a pseudo color; this technique thus allows the facile delineation of different inner organs of the mouse, including the lungs, the kidneys, and the skin (Figure 3d).

The various regions of the mouse body were studied in detail by imaging at higher magnifications (see the Supporting Information). The hindlimb region was imaged in both the 1100–1700 nm and the 1300–1700 nm regions using different long-pass filters, and the resulting images were compared to an image taken in the traditional NIR-I region (ca. 800 nm; Figure 4a). Although the emission of IR-PEG nanoparticles in water peaks at 1064 nm upon 808 nm excitation (Figure 2b), a substantial amount of emission can be still detected at wavelengths longer than 1100 nm or even 1300 nm; in these regions, improved imaging resolution was obtained because of reduced photon scattering by the tissue. The image taken in the traditional NIR window at approximately 800 nm with IRDye 800 showed the features of the mouse hindlimb vasculature only in a blurred fashion, owing to a high degree of photon scattering in the short-wavelength NIR-I window (Figure 4a).[11] In strong contrast, NIR-II imaging in both the 1100–1700 nm and the 1300–1700 nm regions afforded much clearer images of the mouse hindlimb blood vessels, including a delineation of the parallel femoral artery and the vein located in the middle of the hindlimb (Figure 4b,c). A fluorescence image of the mouse hindlimb in the 1100–1700 nm NIR-II region using single-walled carbon nanotubes[11] was also taken (Figure 4e); it exhibits a spatial resolution of the blood vessels similar to that of the fluorescence image with IR-PEG nanoparticles (Figure 4b), which suggests that our new NIR-II fluorophores could achieve an imaging quality that is comparable to that of previously reported NIR-II fluorophores.[11] A negative control image of the mouse hindlimb without injection of any fluorophore was also taken in the 1100–1700 nm NIR-II region (Figure 4f), which shows negligible interference of the NIR-II fluorescence with intrinsic autofluorescence of the mouse body. The abdominal region was also imaged in the 1300–1700 nm NIR-II region; rich blood vessels were observed, with the smallest discernible vessels measured to be approximately 150 μm wide (Figure 4d). The NIR-II fluorescence images clearly reveal vascular structures located at distances >1 mm underneath the skin,[11] owing to much reduced photon scattering at longer wavelengths, as photon scattering in turbid biological tissues is inversely proportional to the wavelength (ca. λ^{-w}; $w = 0.22$–1.68).[10] Much weaker fluorescence was observed one day after the intravenous injection of IR-PEG nanoparticles, and a high fluorescence intensity was detected mainly in the liver (Figure S4). The NIR-II intensity measured for the liver decayed over time, suggesting fecal excretion. None of the mice that were

injected with IR-PEG nanoparticles and used for NIR-II imaging showed any obvious signs of acute poisoning or health problems over about two weeks. Thus, our whole-body video-rate imaging as well as the steady-state imaging of the hindlimb and the abdomen of mice suggested that IR-PEG nanoparticles are biocompatible agents that fluorescence in the >1000 nm region. This allows in vivo imaging with deeper tissue penetration, higher spatial resolution, and better image fidelity than traditional fluorescence imaging in the <900 nm NIR region.

In conclusion, we have developed an NIR-II fluorescent imaging agent for biological systems that is based on a small organic fluorophore. The imaging of inner organs and blood vessels of mice with IR-PEG nanoparticles is the first example of the use of organic molecular fluorophores for in vivo imaging, and matched results with inorganic carbon nanotubes and quantum dots that were previously obtained in the NIR-II region.[10,11] We demonstrated that entrapment of hydrophobic NIR-II organic dyes into an amphiphilic polymeric matrix can lead to improved stability of the organic fluorophores in aqueous solutions, while largely preserving the fluorescence quantum efficiency and imparting biocompatibility for in vivo research. Compared to inorganic materials, including carbon nanotubes, NIR-II agents based on small organic molecules can be much smaller, which leads to more favorable pharmacokinetics, such as efficient tumor targeting and facile excretion. We also compared the IR-PEG particles with previously reported NIR-II fluorescent nanomaterials, including single-walled carbon nanotubes, quantum dots, and rare-earth-metal-doped nanoparticles, in terms of the spectral ranges of their emission and fluorescence quantum yields. The NIR fluorescence spectrum of IR-PEG nanoparticles exhibited fluorescence emission peaks at shorter wavelengths (920 nm and 1064 nm) than previously reported NIR-II fluorophores, such as single-walled carbon nanotubes (multiple emission peaks around 1000–1400 nm with a fluorescence QY of ca. 0.4%, measured against the reference IR-26),[11] Ag_2S quantum dots (one fluorescence emission peak at 1200 nm, QY ca. 15.5%, measured against IR-26),[17] and rare-earth nanoparticles (tunable NIR fluorescence from 1100 nm to 1500 nm with measured quantum efficiencies of up to 1.2%[20] using the absolute integrating-sphere method). Much work lies ahead in synthesizing organic fluorophores that are stable under aqueous conditions and biocompatible without the need for polymer entrapment. The synthesis of small molecules with >1000 nm fluorescence emission could lead to much higher quantum efficiencies, and enable controlled tuning of the excitation and emission wavelengths. Such small organic fluorophores could also be rapidly excreted out of the body, resulting in reduced toxicity problems. With these advances, the development of NIR-II fluorescent agents for wide-spread pre-clinical research and clinical use may be achieved.

Received: August 21, 2013
Revised: September 24, 2013
Published online: October 31, 2013

Keywords: fluorescence · imaging agents · nanoparticles · near infrared · polymers

[1] V. Pansare, S. Hejazi, W. Faenza, R. K. Prud'homme, *Chem. Mater.* **2012**, *24*, 812 – 827.
[2] E. I. Altinoğlu, J. H. Adair, *Wiley Interdiscip. Rev. Nanomed. Nanobiotechnol.* **2010**, *2*, 461 – 477.
[3] R. B. Mujumdar, L. A. Ernst, S. R. Mujumdar, C. J. Lewis, A. S. Waggoner, *Bioconjugate Chem.* **1993**, *4*, 105 – 111.
[4] Y. Lin, R. Weissleder, C. H. Tung, *Bioconjugate Chem.* **2002**, *13*, 605 – 610.
[5] C. Bouteiller, G. Clavé, A. Bernardin, B. Chipon, M. Massonneau, P. Y. Renard, A. Romieu, *Bioconjugate Chem.* **2007**, *18*, 1303 – 1317.
[6] B. Ebert, B. Riefke, U. Sukowski, K. Licha, *J. Biomed. Opt.* **2011**, *16*, 066003.
[7] B. E. Schaafsma, J. S. Mieog, M. Hutteman, J. R. van der Vorst, P. J. Kuppen, C. W. Löwik, J. V. Frangioni, C. J. van de Velde, A. L. Vahrmeijer, *J. Surg. Oncol.* **2011**, *104*, 323 – 332.
[8] K. Welsher, Z. Liu, S. P. Sherlock, J. T. Robinson, Z. Chen, D. Daranciang, H. Dai, *Nat. Nanotechnol.* **2009**, *4*, 773 – 780.
[9] J. T. Robinson, K. Welsher, S. M. Tabakman, S. P. Sherlock, H. Wang, R. Luong, H. Dai, *Nano Res.* **2010**, *3*, 779 – 793.
[10] K. Welsher, S. P. Sherlock, H. Dai, *Proc. Natl. Acad. Sci. USA* **2011**, *108*, 8943 – 8948.
[11] G. Hong, J. C. Lee, J. T. Robinson, U. Raaz, L. Xie, N. F. Huang, J. P. Cooke, H. Dai, *Nat. Med.* **2012**, *18*, 1841 – 1846.
[12] H. Yi, D. Ghosh, M. H. Ham, J. Qi, P. W. Barone, M. S. Strano, A. M. Belcher, *Nano Lett.* **2012**, *12*, 1176 – 1183.
[13] J. T. Robinson, G. Hong, Y. Liang, B. Zhang, O. K. Yaghi, H. Dai, *J. Am. Chem. Soc.* **2012**, *134*, 10664 – 10669.
[14] S. Diao, G. Hong, J. T. Robinson, L. Jiao, A. L. Antaris, J. Z. Wu, C. L. Choi, H. Dai, *J. Am. Chem. Soc.* **2012**, *134*, 16971 – 16974.
[15] A. L. Antaris, J. T. Robinson, O. K. Yaghi, G. Hong, S. Diao, R. Luong, H. Dai, *ACS Nano* **2013**, *7*, 3644 – 3652.
[16] G. Hong, J. T. Robinson, Y. Zhang, S. Diao, A. L. Antaris, Q. Wang, H. Dai, *Angew. Chem.* **2012**, *124*, 9956 – 9959; *Angew. Chem. Int. Ed.* **2012**, *51*, 9818 – 9821.
[17] Y. Zhang, G. Hong, Y. Zhang, G. Chen, F. Li, H. Dai, Q. Wang, *ACS Nano* **2012**, *6*, 3695 – 3702.
[18] W. Liu, A. Y. Chang, R. D. Schaller, D. V. Talapin, *J. Am. Chem. Soc.* **2012**, *134*, 20258 – 20261.
[19] B. Dong, C. Li, G. Chen, Y. Zhang, Y. Zhang, M. Deng, Q. Wang, *Chem. Mater.* **2013**, *25*, 2503 – 2509.
[20] D. J. Naczynski, M. C. Tan, M. Zevon, B. Wall, J. Kohl, A. Kulesa, S. Chen, C. M. Roth, R. E. Riman, P. V. Moghe, *Nat. Commun.* **2013**, *4*, 2199.
[21] J. R. Kanofsky, P. D. Sima, *Photochem. Photobiol.* **2000**, *71*, 361 – 368.
[22] P. Prosposito, M. Casalboni, F. De Matteis, M. Glasbeek, A. Quatela, E. van Veldhoven, H. Zhang, *J. Lumin.* **2001**, *94 – 95*, 641 – 644.
[23] P. Prosposito, M. Casalboni, F. De Matteis, A. Quatela, M. Glasbeek, E. van Veldhoven, H. Zhang, *J. Sol-Gel Sci. Technol.* **2003**, *26*, 909 – 913.
[24] M. Casalboni, F. De Matteis, P. Prosposito, A. Quatela, F. Sarcinelli, *Chem. Phys. Lett.* **2003**, *373*, 372 – 378.
[25] S. C. Farmer, T. E. Patten, *Chem. Mater.* **2001**, *13*, 3920 – 3926.
[26] K. Li, J. Pan, S. S. Feng, A. W. Wu, K. Y. Pu, Y. T. Liu, B. Liu, *Adv. Funct. Mater.* **2009**, *19*, 3535 – 3542.
[27] K. Park, S. Lee, E. Kang, K. Kim, K. Choi, I. C. Kwon, *Adv. Funct. Mater.* **2009**, *19*, 1553 – 1566.
[28] S. Acharya, S. K. Sahoo, *Adv. Drug Delivery Rev.* **2011**, *63*, 170 – 183.
[29] X. Wang, S. Xu, W. Xu, *Nanoscale* **2011**, *3*, 4670 – 4675.

[30] M. Dossi, R. Ferrari, L. Dragoni, C. Martignoni, P. Gaetani, M. D'Incalci, M. Morbidelli, D. Moscatelli, *Macromol. Mater. Eng.* **2013**, *298*, 771 – 778.
[31] Y. Jin, F. Ye, M. Zeigler, C. Wu, D. T. Chiu, *ACS Nano* **2011**, *5*, 1468 – 1475.
[32] S. A. Hilderbrand, F. Shao, C. Salthouse, U. Mahmood, R. Weissleder, *Chem. Commun.* **2009**, 4188 – 4190.
[33] J. H. Ke, J. J. Lin, J. R. Carey, J. S. Chen, C. Y. Chen, L. F. Wang, *Biomaterials* **2010**, *31*, 1707 – 1715.
[34] L. Xiong, T. Yang, Y. Yang, C. Xu, F. Li, *Biomaterials* **2010**, *31*, 7078 – 7085.
[35] Z. Liu, W. Cai, L. He, N. Nakayama, K. Chen, X. Sun, X. Chen, H. Dai, *Nat. Nanotechnol.* **2007**, *2*, 47 – 52.
[36] J. E. Murphy, M. C. Beard, A. G. Norman, S. P. Ahrenkiel, J. C. Johnson, P. Yu, O. I. Mićić, R. J. Ellingson, A. J. Nozik, *J. Am. Chem. Soc.* **2006**, *128*, 3241 – 3247.
[37] O. E. Semonin, J. C. Johnson, J. M. Luther, A. G. Midgett, A. J. Nozik, M. C. Beard, *J. Phys. Chem. Lett.* **2010**, *1*, 2445 – 2450.
[38] E. M. Hillman, A. Moore, *Nat. Photonics* **2007**, *1*, 526 – 530.

